J. Electrochem. Sci. Eng. **16** (2026) 3320; https://doi.org/10.5599/jese.3320

Open Access : : ISSN 1847-9286
https://pub.iapchem.org/ojs/index.php/JESE

Original scientific paper

A newly designed nano metal-organic framework of yttrium-benzenetricarboxylic acid: synthesis, characterization, antimicrobial and electrochemical properties

Sarah Mohammed Mohsin✉, Zeina Haider Abbas, Saja Haider Fadhil and Noor Kareem Aead

Department of Clinical Laboratory Sciences, College of Pharmacy, University of Kerbala, Iraq

Corresponding Author: ✉sarah.mohammed@uokerbala.edu.iq

Received: March 4, 2026; Accepted: April 29, 2026; Published: June 27, 2026

Abstract

In this work, a metal-organic framework based on yttrium and benzene tricarboxylic acid (Y-BTC-MOF) was synthesized via solvothermal synthesis. Y-BTC-MOF was characterized using energy-dispersive X-ray spectroscopy, field emission scanning electron microscopy, X-ray diffraction pattern, Fourier transform infrared spectroscopy, transmission electron microscopy and an elemental mapping image. Also, Y-BTC-MOF was applied for the modification of a screen-printed electrode. The modified electrode was used for voltammetric determination of doxorubicin in the calibration range of 0.002 to 110.0 µM.

Keywords

Doxorubicin drug, screen printed electrode, chemical modification; functional porous materials; antibacterial tests, biological real samples

Introduction

Cancer is the most common life-threatening illness that raises morbidity and mortality rates worldwide. It is a terrible disease that has long been a major contributor to human mortality [1]. Anti-neoplastic drugs affect both cancerous and healthy cells by preventing or eradicating cell proliferation [2]. Drug analysis is an important method for guaranteeing the quality of medications. Developing a drug detection method that is easy to use, sensitive, fast, and dependable is essential [3].

The anthracycline drug doxorubicin (DOX), sometimes referred to as adriamycin, is widely used to treat a variety of cancers. In disseminated neoplastic diseases such as carcinoma, neuroblastoma, leukaemia, and sarcomas, it causes regression [4]. Its therapeutic use is restricted by several harmful effects on neo-plastic cells [4]. Therefore, it is crucial to develop highly sensitive analytical methods to detect traces of doxorubicin in clinical therapy. Doxorubicin can be found using liquid chromatography, electrochemical sensors, electrophoresis, and fluorimetry [5]. Because of their instrumental simplicity,

affordability, and portability, the authors are primarily considering electrochemical procedures among the aforementioned approaches for detecting the analytes. There is sufficient evidence to conclude that the inert surface kinetics of ordinary electrodes pose substantial problems that negatively impact the electrode's sensitivity and selectivity [6-8].

One relatively new technique for improving analyte-surface interactions is electrode surface modification [9]. Because of their low background current, ease of surface renewal, broad range of possible windows, lower detection limit, and affordability, chemically modified electrodes have garnered significant attention in the study of numerous species [10]. Nanomaterials have attracted considerable interest due to their unique properties and strong potential for use in the development of nanodevices [10]. Nanomaterials have potential uses in electrochemical sensors to improve electron transit between the electrode surface and the electrolyte because of their high surface area, good conductivity, and superior catalytic activity [11].

Metal-organic frameworks (MOFs), which self-assemble from organic linkers and metal ions, have attracted considerable attention due to their exceptionally large surface area, tunable functionality, and diverse pore topologies [12]. Depending on the intended use, MOFs can be constructed as a variety of networks with diverse chemical and physical properties. MOFs have recently been shown to be a unique material to replace the electrode for electrochemical applications [13].

Because they can be produced in large quantities at low cost and are disposable, screen-printed carbon electrodes (SPCEs) are a good option for point-of-care devices [14]. However, one drawback of SPCEs is that the researcher (customer) is typically unaware of the commercial ink formulations, which contain non-conducting binders [15]. The background currents of these electrodes can be substantial and limit detection limits in practical devices. The varied ink components might influence the electrochemical characteristics in different ways. Lastly, different electrode devices may have very different surface electrochemical characteristics [16-18].

Y-BTC-MOF nanocomposite was employed as a modifier to alter the SPE in the current study. We used cyclic voltammetry (CV), chronoamperometry, and differential pulse voltammetry (DPV) to examine the electrochemical characteristics of DOX after changing the SPE. Under optimal experimental conditions, the proposed electrode exhibited impressive catalytic activity for the DOX redox process. Furthermore, the current approach reliably and accurately identifies DOX in actual samples.

Experimental

Chemicals and instrumentations

Merck and Sigma-Aldrich solvents and chemicals were used without further purification.

A Shimadzu-470 spectrometer with a CsI disk in the range of 4000 to 250 cm^{-1} was used to record the Fourier transform infrared (FT-IR) spectra at 1 % dispersion. An expert diffractometer (Advance D8, Germany) using copper Kα radiation was used to collect the X-ray diffraction (XRD) data. At 298 K, the sample was scanned between 2θ= 10 and 80°. The EM8000F scanning electron microscope (Kyky, China) was used to obtain field-emission scanning electron microscopy (FE-SEM) images. Philips em208s, 100 kV, was used for the transmission electron microscopy (TEM) studies.

Gentamicin and amikacin were used as references, an incubator manufactured by Shimaz Company and a spectrophotometer Optizen 2120 UV plus made in Korea were used in antibacterial studies.

The electrochemical measurements were carried out using an Autolab PGSTAT 302 N potentiostat/galvanostat. Three standard electrodes make up the SPE (DropSens, DRP-110, Spain): an unaltered graphite working electrode, a silver pseudo-reference electrode and a graphite counter electrode.

Synthesis of nano metal-organic framework of yttrium-benzene tricarboxylic acid

The following process was used to synthesize Y-BTC-MOF. First, the solution was prepared by dissolving 0.80 mmol (0.30 g) of $Y(NO_3)_3{\cdot}6H_2O$ in 30 mL of C_2H_5OH. Next, 1.2 mmol (0.25 g) of benzene tricarboxylic acid (BTC) was combined with 30 mL of ethanol to prepare solution II. After that, the solution I and II mixture was refluxed for six hours. Y-BTC-MOF crystals developed after 24 h.

To create Y-BTC-MOF at the nanoscale, 0.50 mM of MOF was dissolved in 25 mL of DMF solution. After that, it was ultrasonicated for roughly half an hour. Following that, these compounds underwent a solvothermal reaction in an autoclave that was heated to 120 °C for 48 h. The precipitates were collected after the solvothermal reaction was complete and the autoclave had cooled to room temperature. The obtained precipitates were then repeatedly cleaned with DMF and ethanol and dried overnight at 100 °C to yield Y-BTC-MOF.

Preparation of the modified electrode

A straightforward procedure was used to coat the unmodified SPE with Y-BTC-MOF: 1 mg of Y-BTC-MOF was dissolved in 1 mL of water and ultrasonicated for 25 minutes. The surface of the working electrode was then covered with 3 µL of the constructed suspension. It was dried at ambient temperature.

The real samples

The urine samples were first centrifuged for 600 seconds at 10 mL each. Following that, various volumes of the treated urine samples were collected, placed in flasks, and diluted with a pH 7.0 phosphate buffer (PB) solution. These samples were treated with varying concentrations of doxorubicin (DOX). The conventional addition method is used to measure the DOX concentrations.

The DOX ampoule was mixed with 10 mL of PB. A series of 25 mL volumetric flasks was filled with varying quantities of the resulting diluted solution. The conventional addition method was used for the analysis.

Results and discussion

Physical characterization of nano metal-organic framework of yttrium-benzene tricarboxylic acid

The functional groups in the Y-BTC-MOF structure were examined using FT-IR spectroscopy. Figure 1 displays the equivalent FT-IR spectrum.

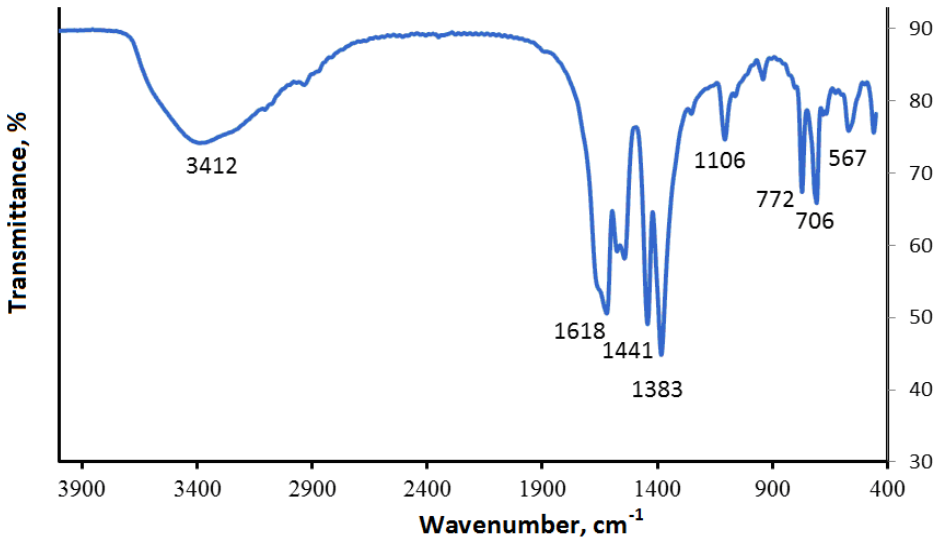

Figure 1. *FT-IR spectrum of Y-BTC-MOF*

The stretching vibrations of the Y-O bond are probably responsible for the apparent peak in this spectrum at 567 cm^{-1}. The band at 1106 cm^{-1} represents the in-plane bending vibration of C-H, whereas the bands at 706 and 772 cm^{-1} represent vibration of C-H. The vibrations of the aromatic ring of C=C were identified as the cause of the designated peak at 1441 cm^{-1}. Y is coordinated with the carboxylate groups. The spectrum shows peaks at 1541 cm^{-1} and 1618 cm^{-1} for the symmetric stretching vibration, and the peak at 1119 cm^{-1} is associated with the asymmetric stretching vibration of (COO-) [19]. The hydroxyl group of Y-BTC MOF exhibits a stretching vibration at 3412 cm^{-1} [20,21].

Y-BTC's XRD pattern (Figure 2), which matched the previously published data [22], showed distinctive peaks at 2θ = 8.65, 10.62, 13.71, 17.33, 18.35, 20.35, 22.98, 26.82, 27.57 and 36.78°.

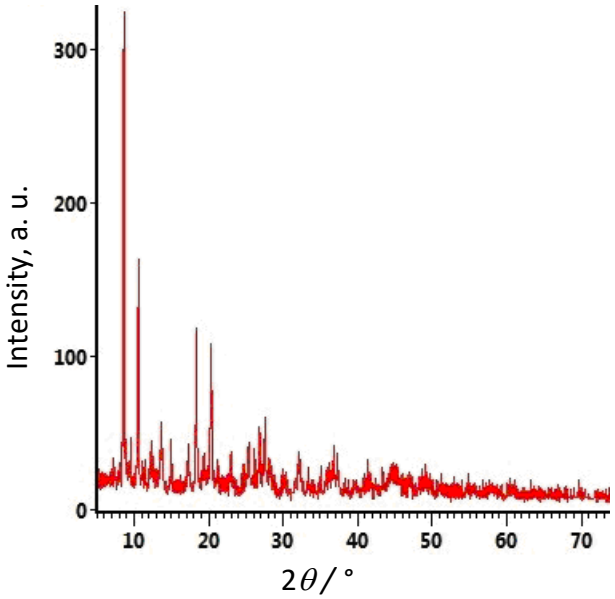

Figure 2. *XRD patern of the synthesized MOF*

Figure 3 displays FE-SEM pictures of the MOF. The SEM images show that the Y-BTC-MOF crystals have flat surfaces and are spherical and rod-shaped.

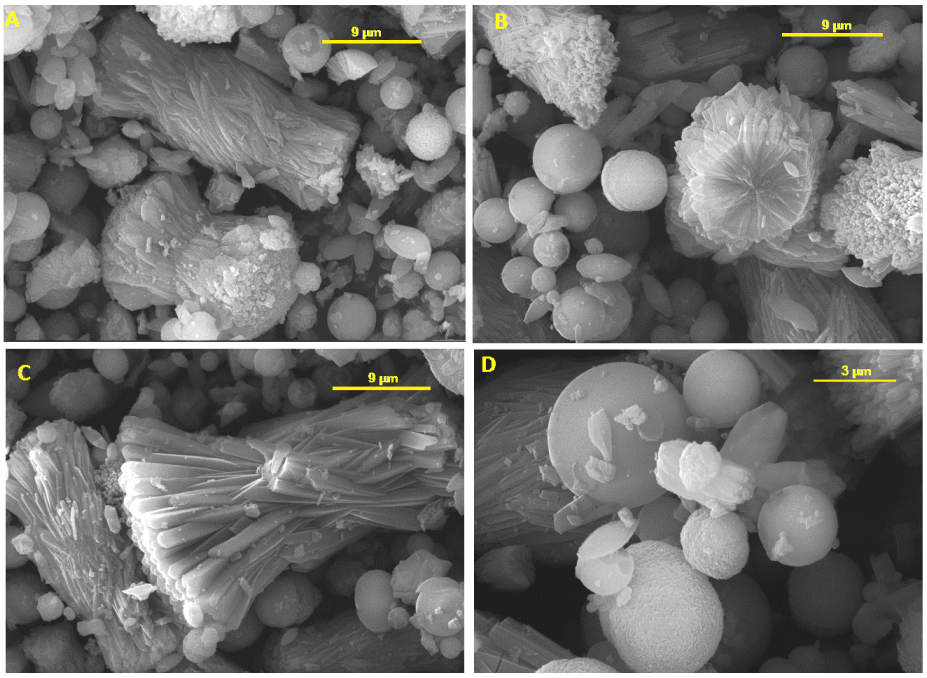

Figure 3. *FE-SEM images of MOF*

The elements found in Y-BTC MOF were verified by energy-dispersive X-ray spectroscopy (EDS) (Figure 4). The production of Y-BTC-MOF was verified by the presence of Y, C and O.

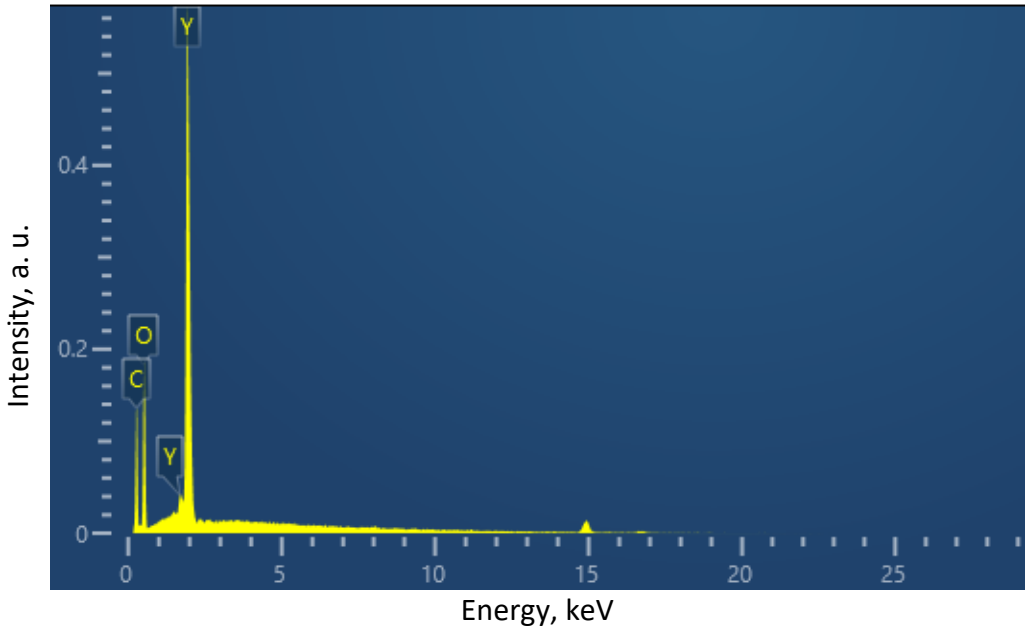

Figure 4. *EDS spectrum of MOF*

The EDS mapping images of O, C and Y in the MOF are shown in Figure 5.

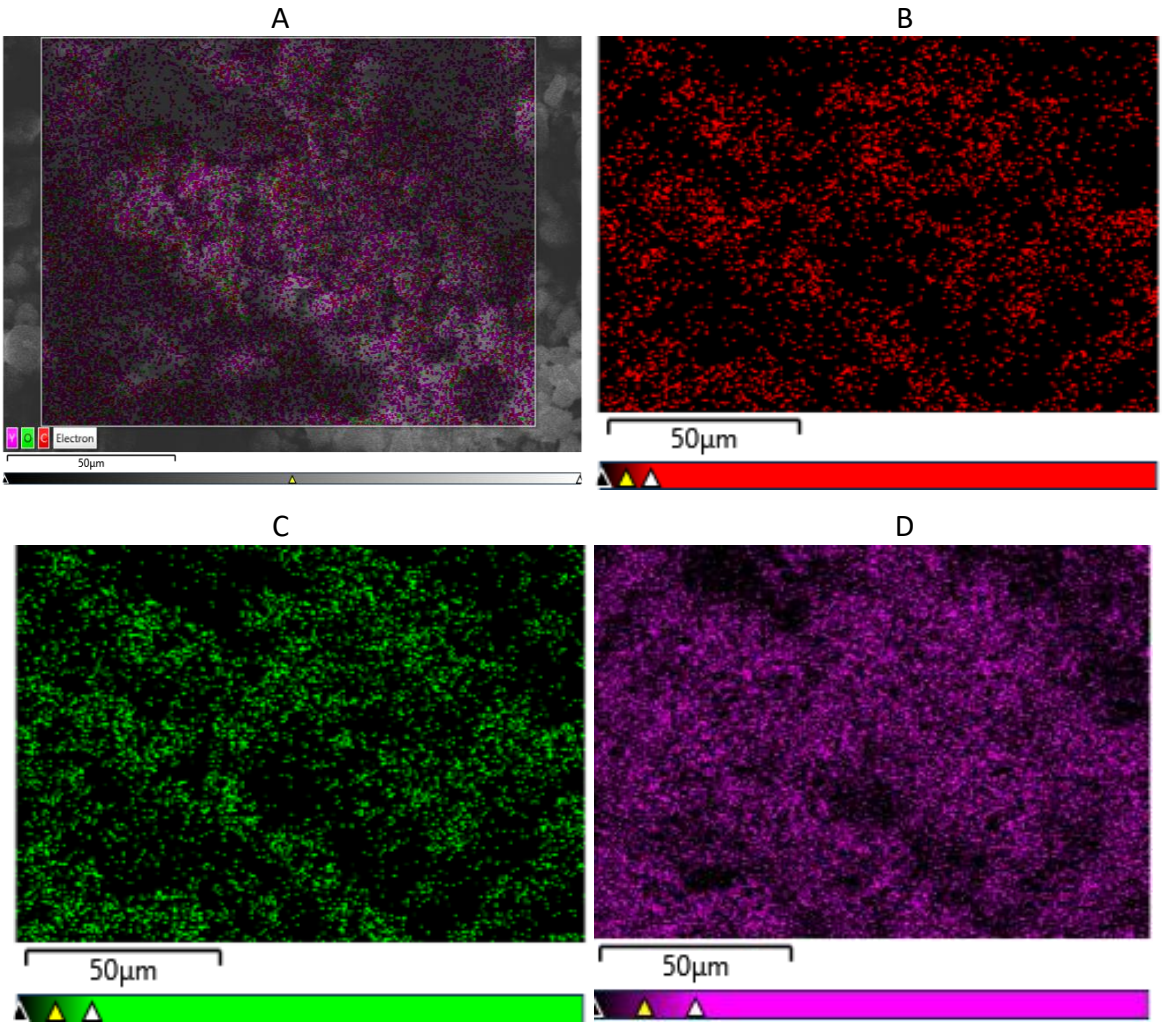

Figure 5. *EDS mapping images of A - MOF; and B - oxygen, C - carbon and D -yttrium*

http://doi.org/10.5599/jese.3320

TEM examination was used to look at the morphology and particle size of the as-synthesised Y-BTC-MOF. Y-BTC-MOF TEM pictures show the buildup of smooth-surfaced crystals. The nano-particles were effectively integrated into the Y-BTC form, as demonstrated by the TEM image of Y-BTC-MOF (Figure 6).

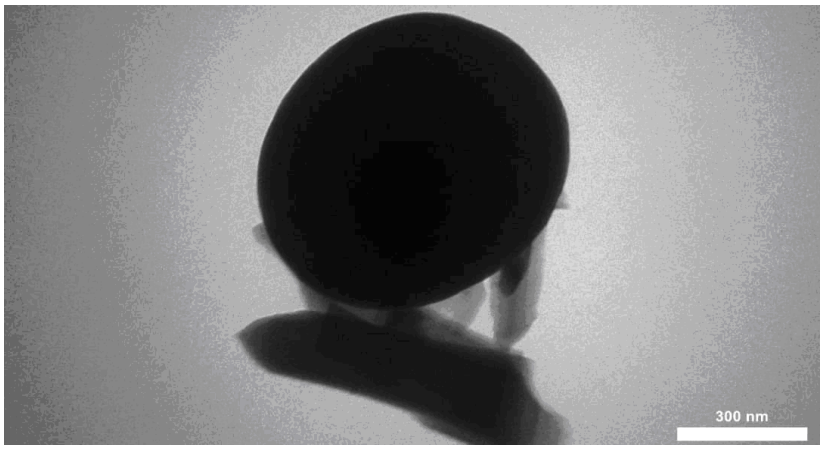

Figure 6. *TEM image of Y-BTC-MOF*

Electrochemical oxidation of doxorubicin at the surface of nano metal-organic framework of yttrium-benzene tricarboxylic acid/screen printing electrode

The pH has a significant impact on DOX's electrochemical behaviour. Therefore, adjusting the pH was a crucial step. To this goal, CV tests were carried out using 0.1 M PB solutions (pH 2.0 to 9.0). The results demonstrated that the oxidation of DOX favours neutral pH. Based on the data, the ideal pH was determined to be 7.0 and used in all experiments.

Figure 7 displays the CVs obtained using the bare (graph a) and modified (graph b) SPEs. The greatest oxidation of DOX on the Y-BTC-MOF/SPE occurs around 450 mV, which is roughly 60 mV more negative than unmodified SPE, according to CV findings. Y-BTC-MOF's increased surface area and the notable electron-transfer capabilities of nanomaterials are responsible for the enhanced electrochemical catalytic activity of Y-BTC-MOF/SPE.

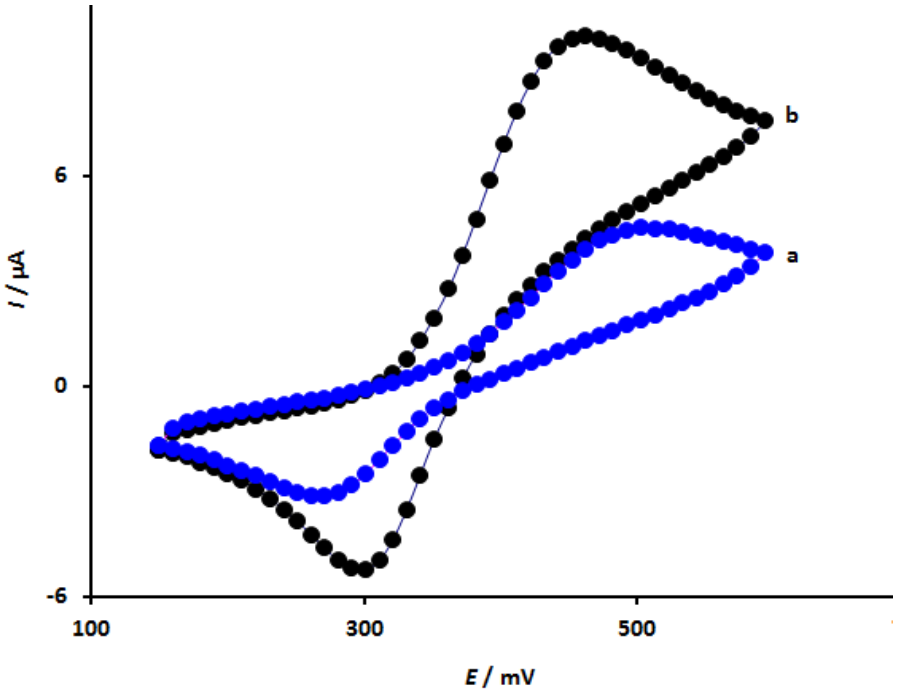

Figure 7. *CVs of a) unmodified SPE and b) Y-BTC-MOF/SPE in 30.0 µM DOX. The scan rate was 50 mV* s^{-1}

Therefore, the DOX electron transfer was greatly enhanced by Y-BTC-MOF/SPE. Furthermore, Y-BTC-MOF/SPE exhibits much larger anodic peak currents for DOX oxidation than the unmodified SPE, suggesting that the electrode's performance toward DOX oxidation has been greatly enhanced by the addition of Y-BTC-MOF to the unmodified SPE.

Effect of scan rate

It has been investigated how potential sweep rates affect the redox current of DOX (Figure 8). The linear dependence of the anodic and cathodic peak currents on $v^{1/2}$ over a broad range indicates that the oxidation and reduction processes are diffusion-controlled (Figure 8A).

Plotting the log I_{pa} against the log v produced a straight line with a slope of 0.5619 (Figure 8B), which is near the theoretical value of 0.5 for a process that is solely diffusion controlled. This further confirms that the process is diffusion-controlled.

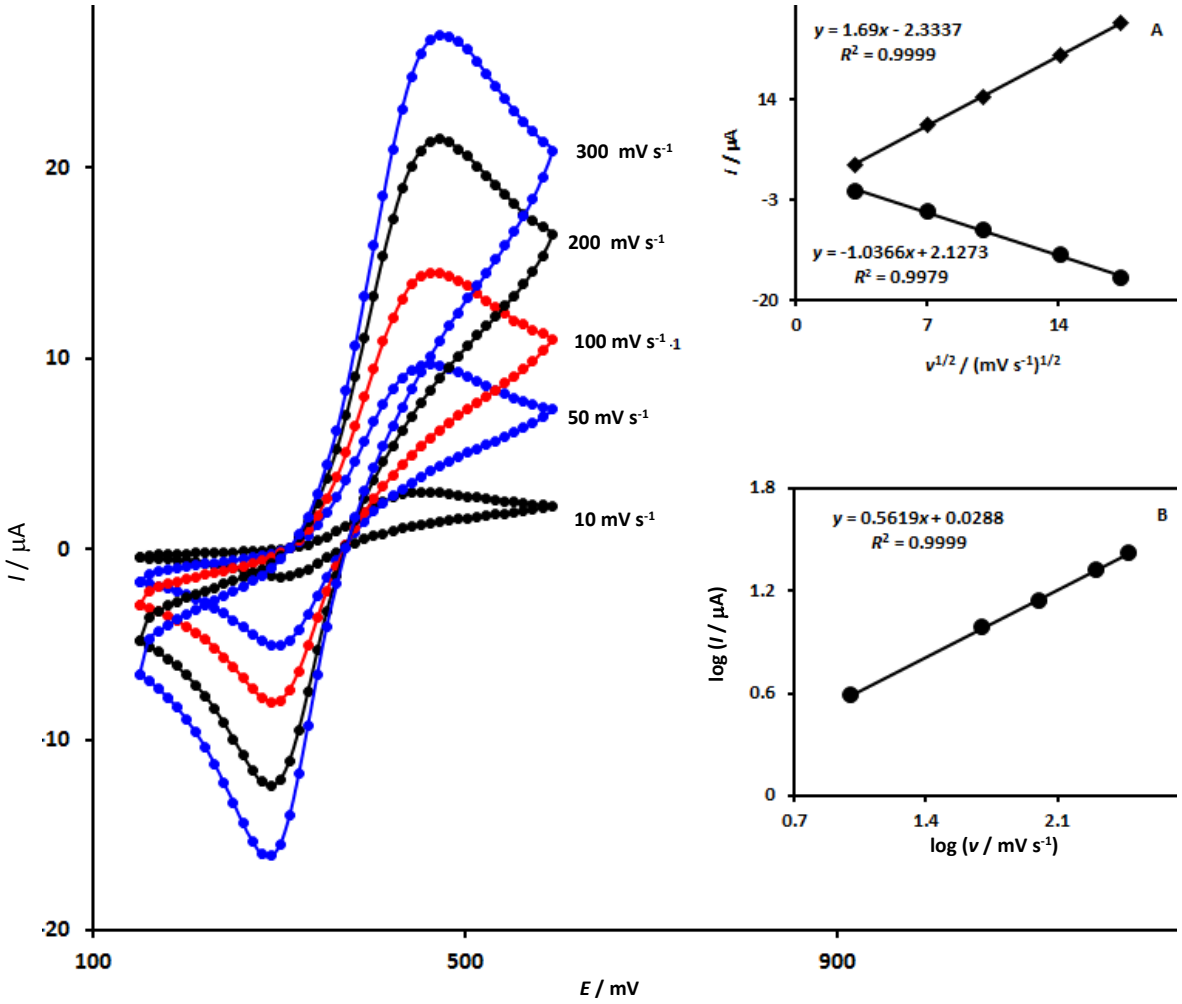

Figure 8. *CVs of Y-BTC-MOF/SPE at different scan rates in 30.0 µM DOX. Inset: (A) anodic and cathodic peak current variation* vs. $v^{1/2}$ *and (B) relationship between log* I_{pa} *and log v*

Chronoamperometric studies

The electrode potential was set at 500 mV for different DOX concentrations in PB (pH 7.0) to perform chronoamperometric studies of DOX at Y-BTC-MOF/SPE (Figure 9) and to apply the Cottrell equation. Plots of *I vs.* $t^{-1/2}$ are shown in Figure 10A. The value of *D* was determined to be 5.48×10^{-5} cm^2 s^{-1} using the Cottrell equation and the slope shown in Figure 10B.

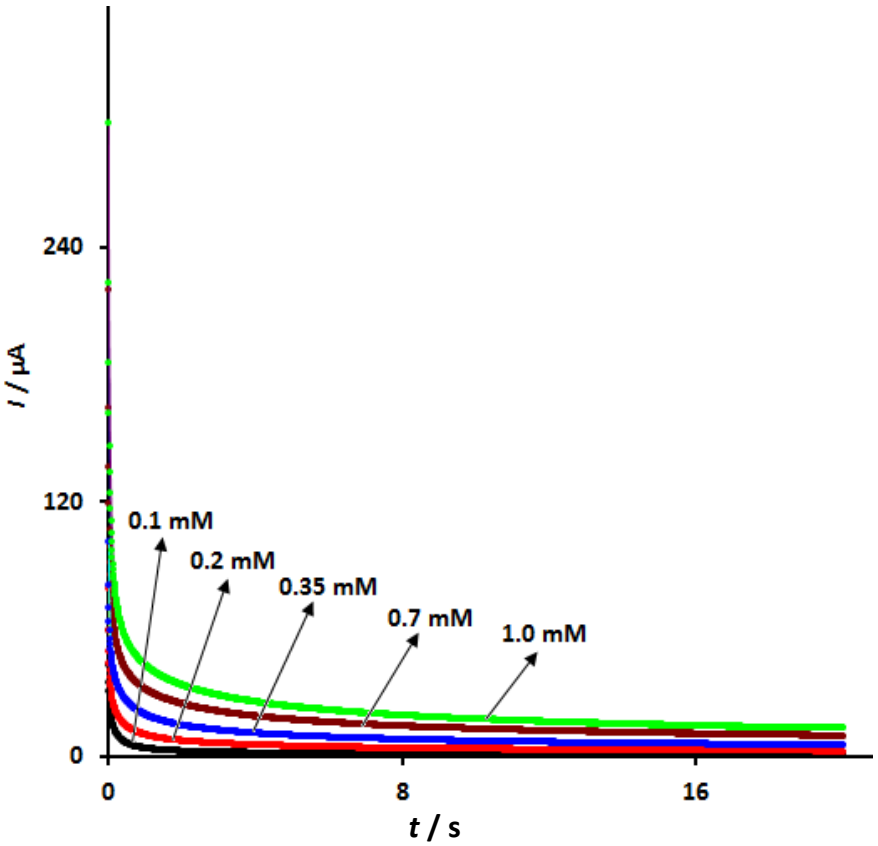

Figure 9. *Chronoamperograms obtained at Y-BTC-MOF/SPE in 0.1 M PB (pH 7.0) for different concentrations of DOX (0.1 to 1.0 mM)*

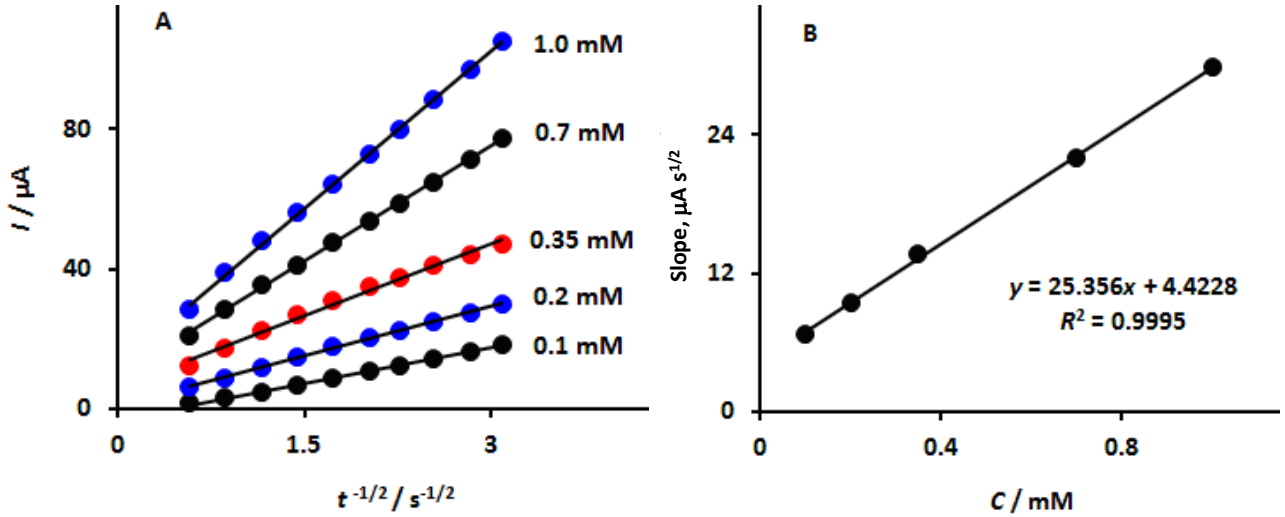

Figure 10. *A - plots of current* vs. $t^{-1/2}$*, B - plot of the slopes in A against DOX concentration*

Calibration curve

Tests using differential pulse voltammetry (DPV) were conducted at various DOX doses (Figure 11). The peak current of DOX increased linearly from 0.002 to 110.0 µM. The limit of detection (LOD) for DOX was computed from the calibration curve using the following formula: LOD = 3 S_b/m, where m represents the slope of the calibration graph and standard deviation (S_b) was computed for an intercept (n = 5). The LOD was found to be 0.001 µM.

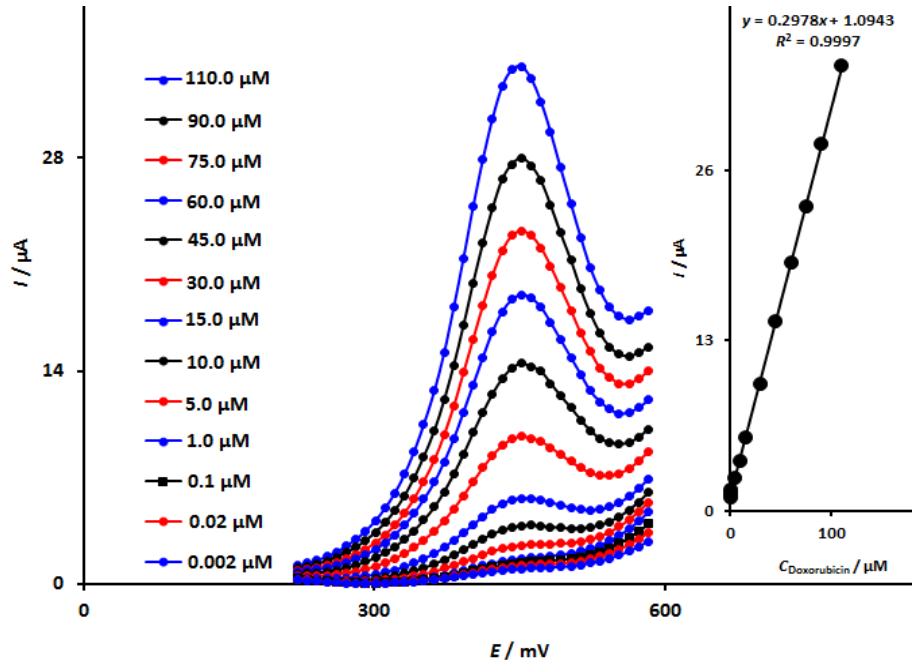

Figure 11. *DPVs of Y-BTC-MOF/SPE in different concentrations of DOX (0.002 to 110 µM). Inset: I_{peak} vs. DOX concentration*

Analysis of real samples

The modified electrode was used to determine DOX in urine and injection samples to assess its suitability for real analytical applications (Table 1). These findings demonstrate satisfactory DOX recoveries. Relative standard deviation (RSD) was used to express the DOX's repeatability.

Table 1*. Application of Y-BTC-MOF/SPE for concurrent determination of DOX in urine and DOX injection samples (*n*=5)*

Sample	Spiked, µM	Found, µM	Recovery, %	RSD, %
DOX injection	0	3.4	-	3.2
	2.0	5.3	98.1	1.8
	4.0	7.6	102.7	2.7
	6.0	9.5	101.1	2.5
	8.0	11.3	99.1	2.9
Urine	5.0	5.1	102.0	2.2
	7.0	6.8	97.1	3.5
	9.0	8.9	98.9	1.9
	11.0	11.4	103.6	2.6

In-vitro anti-microbial experiment

The anti-bacterial activity of the Y-BTC MOF was tested on two Gram-negative members, *Escherichia coli* (*E. coli* ATCC 25922) and *Pseudomonas aeruginosa* (*P. aeruginosa* ATCC 27853), as well as two Gram-positive members, *Staphylococcus aureus* (*S. aureus* ATCC 25923) and *Enterococcus faecalis* (*Enter_faeca* ATCC 29212). Here, the minimum bactericidal concentration (MBC) and minimum inhibitory concentration (MIC) of the complex produced were determined using the broth macro-dilution technique (Table 2).

Additionally, the disk diffusion method was used to calculate the diameter of the expanded inhibition zone (IZ) near the cavity. The MIC is the lowest concentration of an antibiotic molecule that, during a 24-hour incubation period, significantly inhibits bacterial growth at 310 K. DMSO and distilled water were used to create the Y-BTC MOF stock solution.

Table 2. *MIC and MBC of $Y(NO_3)_3{\cdot}6H_2O$, benzenetricarboxylic acid and Y-BTC MOF (in mg mL^{-1}) against investigated bacterial strains*

Bacterial strain	$Y(NO_3)_3{\times}6H_2O$		Benzenetricarboxylic acid		Y-BTC MOF	
	MIC	MBC	MIC	MBC	MIC	MBC
Escherichia Coli	0.0125	0.0250	0.0250	0.0250	0.0125	0.0250
Pseudomonas aeruginosa	0.0250	0.0500	Unavailable for the study		0.0125	0.0250
Staphylococcusaureus	0.0125	0.0250	0.0250	0.0500	0.0062	0.0125
Enterococcus faecalis	0.0125	0.0250	Unavailable for the study		0.0030	0.0060

Finally, we measured each bacterial-growth-free IZ's diameter (Table 3). The MIC, MBC, and inhibitory zone tests were run three times, and the average of the results was calculated. In these tests, amikacin and gentamycin were used as traditional, proven antibacterial agents [23,24].

Table 3. *Inhibition zone (mm) for $Y(NO_3)_3{\cdot}6H_2O$, benzenetricarboxylic acid and Y-BTC MOF against investigated bacterial strains*

	Inhibition zone, mm				
	$Y(NO_3)_3{\times}6H_2O$	Benzenetricarboxylic acid	Y-BTC MOF	Gentamycin	Amikacin
Escherichia Coli	18	10	22	19.2	-
Pseudomonas aeruginosa	*	11	24	20.1	-
Staphylococcus aureus	16	13	26	-	18.8
Enterococcus faecalis	*	14	28	-	19.2

*Unavailable for the study

Conclusion

This study successfully fabricated a novel DOX sensor using a modified screen-printed electrode and synthesized a new Y-BTC-MOF. Regarding DOX detection, Y-BTC-MOF has a more favourable electrocatalytic function and a larger surface area. At the Y-BTC-MOF/SPE surface, DOX may offer higher sensitivity than on the unmodified electrode. With a wide linear range, a low limit of detection, and fast response times for DOX determination, the final sensor demonstrated exceptional analytical performance. Additionally, the MBC, MIC and IZ characteristics of the $Y(NO_3)_3$, benzenetricarboxylic acid, and Y-BTC-MOF were used to examine standard strains. The findings confirm that Y-BTC-MOF has much higher antibacterial activity than its $Y(NO_3)_3$ and benzenetricarboxylic acid as a linker.

Funding: *No funding.*

References

[1] C. Calderón-Figueroa, A. Castillo-Delgado, L. Rodriguez-Osiac, E. A. Castellón, K. Puschel, Ó. Arteaga, A. Fuentes-García, Institutional practices for cancer: Comparison of social and health care along disease trajectory in five countries with high survival rates, *Journal of Cancer Policy* 21 (2026) 100733. https://doi.org/10.1016/j.jcpo.2026.100733

[2] D. G. Passey, R. Healy, J. Qualls, A. Halwani, B. C. Sauer, Pharmacist-led collaborative medication management programs for oral antineoplastic therapies: A systematic literature review, *Journal of the American Pharmacists Association* **61** (2021) e7-e18. https://doi.org/10.1016/j.japh.2020.12.005

[3] K. A. Madurani, Y. Triana, A. Wafi, S. R. Sari, S. N. Jenie, N. N. Zain, P. Tiadeka, Graphene innovations: transforming drug detection technologies for clinical and environmental applications, *Microchemical Journal* **17** (2026) 117743. https://doi.org/10.1016/j.microc.2026.117743

[4] M. Qiu, Z. Wang, Y. Teng, M. Li, F. Wu, Y. Tian, Targeting lncRNA-Mediated Networks to Overcome Doxorubicin Resistance in Cancer, *Critical Reviews in Oncology/Hematology* **13** (2026) 105214. https://doi.org/10.1016/j.critrevonc.2026.105214
[5] L. Wang, S. Gu, F. Yan, C. Shen, Rapid determination of liposomal encapsulation efficiency of doxorubicin using an integrated separation-enrichment-sensing electrochemical platform based on bipolar vertically-ordered mesoporous silica nanochannel arrays, *Microchemical Journal* **19** (2025) 116658. https://doi.org/10.1016/j.microc.2025.116658
[6] N. Erk, G. Kurtay, W. Bouali, A. A. Genç, Molecular binding and electrochemical detection synergy: A study on doxorubicin using nanodiamond-glassy carbon electrodes, *Microchemical Journal* **210** (2025) 112907. https://doi.org/10.1016/j.microc.2025.112907
[7] Z. Wang, H. Wang, M. Cao, Y. Liu, Preparation of electrochemical sensor for detection of cancer medicine doxorubicin based on multi-walled carbon nanotube composites modified electrode, *Alexandria Engineering Journal* **93** (2024) 51-58. https://doi.org/10.1016/j.aej.2024.02.067
[8] E. Lulek, J. Soleymani, M. Molaparast, Y. N. Ertas, Electrochemical sensing of doxorubicin hydrochloride under sodium alginate antifouling conditions using silver nanoparticles modified glassy carbon electrodes, *Talanta* **265** (2023) 124846. https://doi.org/10.1016/j.talanta.2023.124846
[9] N. A. Salman, I. A. Jassem, I. N. Taeb, A simple UiO-66-NH_2@ MWCNTs based electrochemical sensor for the sensitive detection of metronidazole, *ADMET & DMPK* **14** (2026) 2940. https://doi.org/10.5599/admet.2940
[10] S. Deepa, B. K. Swamy, K. V. Pai, A surfactant SDS modified carbon paste electrode as an enhanced and effective electrochemical sensor for the determination of doxorubicin and dacarbazine its applications: A voltammetric study, *Journal of Electroanalytical Chemistry* **879** (2020) 114748. https://doi.org/10.1016/j.jelechem.2020.114748
[11] A. Obaid Imarah, N. Hasan, M. G. Alabbasi, ZnO-modified carbon paste electrode for electrochemical sensing of dopamine in the presence of tyrosine, *ADMET & DMPK* **13** (2025) 3010. https://doi.org/10.5599/admet.3010
[12] A. A. Bhoite, N. L. Tarwal, Metal-organic frameworks (MOFs) and their composites as electrode materials for supercapacitor applications, *Sustainable Materials and Technologies* **11** (2026) e01956. https://doi.org/10.1016/j.susmat.2026.e01956
[13] J. Wang, M. Xu, X. Liang, Y. Zhang, D. Yang, L. Pan, W. Fang, C. Zhu, F. Wang, Development of a novel 2D Ni-MOF derived NiO@ C nanosheet arrays modified Ti/TiO_2NTs/PbO_2 electrode for efficient electrochemical degradation of salicylic acid wastewater, *Separation and Purification Technology* **263** (2021) 118368. https://doi.org/10.1016/j.seppur.2021.118368
[14] F. Khazaal, Q. M. Salih, R. Radi Karabat, R. Muslim Muhibes Electrochemical determination of calcium folinate in the presence of methotrexate and 5-fluorouracil using UiO-66/CdS composite modified screen-printed carbon electrode, *ADMET & DMPK* **13** (2025) 2897. https://doi.org/10.5599/admet.2897
[15] M. A. Azzam, A. Ahmad, A. A. Labib, W.A. Mohamed, A. K. El-Sawaf, H. T. Handal, Advanced Screen-Printed Electrodes: Shaping the Future of Electrochemical Wastewater Analysis: A Review, *Electrochimica Acta* **561** (2026) 148646. https://doi.org/10.1016/j.electacta.2026.148646
[16] S. Hong, S. Oh, E. Kim, E. Park, H. C. Chun, I. T. Kim, Y. R. Kim, Fabrication of screen-printed electrodes with long-term stability for voltammetric and potentiometric applications, *Sensors and Actuators Reports* **8** (2024) 100234. https://doi.org/10.1016/j.snr.2024.100234
[17] P. Kelíšková, O. Matvieiev, L. Janíková, R. Šelešovská, Recent advances in the use of screen-printed electrodes in drug analysis: A review, *Current Opinion in Electrochemistry* **42** (2023) 101408. https://doi.org/10.1016/j.coelec.2023.101408

[18] M. Sher, A. Faheem, W. Asghar, S. Cinti, Nano-engineered screen-printed electrodes: A dynamic tool for detection of viruses, *TrAC Trends in Analytical Chemistry* **143** (2021) 116374. https://doi.org/10.1016/j.trac.2021.116374

[19] L. M. Chen, J. Liu, J. C. Chen, S. Shi, C. P. Tan, K. C. Zheng, L. N. Ji, Experimental and theoretical studies on the DNA-binding and spectral properties of water-soluble complex [Ru (MeIm)$_4$ (dpq)]$^{2+}$, *Journal of Molecular Structure* **881** (2008) 156-166. https://doi.org/10.1016/j.molstruc.2007.09.010

[20] E. Sadeghi, N. S. Peighambardoust, S. Chamani, U. Aydemir, Designing in situ grown ternary oxide/2D Ni-BDC MOF nanocomposites on nickel foam as efficient electrocatalysts for electrochemical water splitting, *ACS Materials Au* **3** (2022) 143-163. https://doi.org/10.1021/acsmaterialsau.2c00073

[21] R. Srinivasan, R. Yogamalar, A. Chandra Bose, Synthesis and structural studies on nanocrystalline yttrium oxide, *Advanced Science Letters* **2** (2009) 65-69. https://doi.org/10.1166/asl.2009.001

[22] F. L. Presti, A. Borzì, A. L. Pellegrino, P. Rossi, P. Paoli, G. Malandrino, Morphology controlled synthesis of yttrium metal–organic frameworks with a tritopic ligand, *Results in Chemistry* **4** (2022) 100640. https://doi.org/10.1016/j.rechem.2022.100640

[23] S. M. Tala-Tapeh, N. Mahmoodi, A. Vaziri, Synthesis of bis-chalcones based on 5, 5′-methylenebis (2-hydroxybenzaldehyde) and screening their antibacterial activity, *Journal of Applied Chemistry* **9** (2015) 53-58. https://Chemistry.journals.semnan.ac.ir

[24] A. K. Chatterjee, R. Chakraborty, T. Basu, Mechanism of antibacterial activity of copper nanoparticles, *Nanotechnology* **25** (2014) 135101. https://doi.org/10.1088/0957-4484/25/13/135101